Future Climates from Bias-Bootstrapped Weather Analogs: An Application to the Yangtze River Basin

BORIS ORLOWSKY

Institute for Atmospheric and Climate Science, ETH Zurich, Zurich, Switzerland

OLIVER BOTHE AND KLAUS FRAEDRICH

Meteorological Institute, KlimaCampus, University of Hamburg, Hamburg, Germany

FRIEDRICH-WILHELM GERSTENGARBE

Potsdam Institute for Climate Impact Research, Potsdam, Germany

XIUHUA ZHU

Max Planck Institute for Meteorology, KlimaCampus, Hamburg, Germany

(Manuscript received 2 June 2009, in final form 21 January 2010)

ABSTRACT

The authors describe a statistical analog resampling scheme, similar to the ''intentionally biased bootstrap,'' for future climate projections whose only constraint is a prescribed linear temperature trend. It provides a large ensemble of day-to-day time series of single-station weather variables and other climatological observations at low computational cost. Time series are generated by mapping time sequences from the observed past into the future. The Yangtze River basin, comprising all climatological subregions of central China, is used as a test bed. Based on daily station data (1961–2000), the bootstrap scheme is assessed in a cross-validation experiment that confirms its applicability. Results obtained for the projected future climates (2001–40) include climatological profiles along the Yangtze, annual cycles, and other weather-related phenomena (e.g., floods, droughts, monsoons, typhoons): (i) the annual mean temperature and, associated with that, precipitation increase; (ii) the annual cycle shows an extension of the Asian summer monsoon season with increasing rainfall, linked to a small summer temperature reduction in the Yangtze lower reaches; (iii) coupling between monsoon circulation and monsoon rainfall strengthens; (iv) while drought occurrence is reduced, Yangtze floods do not change considerably; and (v) the number of typhoon days in the East China Sea shows a reduction of about 25%; the proportion of intense typhoons with landfall increases. GCM scenario simulations produce similar results.

1. Introduction

For future climate projections at a regional scale, a hierarchy of dynamical models is commonly used to simulate the physical processes of the climate system at different spatiotemporal scales and resolutions. In this hierarchy, the coarse-resolution global scale is covered by coupled ocean–atmosphere general circulation models (GCMs). For the regional scale, thanks to an increasing understanding of finescale processes such as cloud formation and growing computer power, the nesting of regional climate models (RegCMs) into GCMs has become a standard approach, despite the large computational costs involved. Regional climate simulations obtained from such a model hierarchy have improved considerably over the last 15 years (Solomon et al. 2007, chapter 11; Wang et al. 2004; Giorgi 2006; Laprise 2008). Such progress is essential for the study of climate impacts that concern single regions rather than the entire globe. Since RegCMs simulate the physical processes entailing regional climate change, they allow for insights into the interplay between causes and consequences. This is of particular importance for simulations of the distant future when climate is expected to be fundamentally different from present-day conditions (Solomon et al. 2007, chapter 10).

Corresponding author address: Boris Orlowsky, Institute for Atmospheric and Climate Science, ETH Zurich, Universitätsstr. 16, 8092 Zurich, Switzerland.
E-mail: boris.orlowsky@env.ethz.ch

DOI: 10.1175/2010JCLI3271.1

However, for certain regions, boundary conditions such as topography or finescale physical processes such as convection still have too coarse of a representation in the RegCMs. In these cases, control simulations from RegCMs are biased against observations (Giorgi et al. 2004; Kotlarski et al. 2005), which limits their use for near-future regional climate impact studies requiring reliable predictive skills. To address this problem, statistical schemes complementing the RegCMs are used, which are less affected by the aforementioned bias problems.

Examples of such statistical schemes are regression models (not unlike the classical model output statistics from the 1960s), analog methods (Wilby et al. 1998; Zorita and von Storch 1999), and stochastic weather generators (Wilks 1999). Regression models exploit statistically derived relations between GCM output and regional weather. Analog methods typically search the past circulation pattern that is most similar to the pattern of a future date (simulated by a GCM) and assign the regional weather concurrent of that past pattern to the future pattern date. Thus, the obtained future combinations of regional weather variables are physically consistent at each time step. Both regression and analog methods downscale GCM output at individual time steps. This makes the skill of their projections dependent on the skill of single GCM runs, which is known to be low for certain regions and variables [see van Oldenborgh et al. (2009); Vautard et al. (2009) for studies revealing underestimated temperature trends over western Europe in GCM simulations].

Stochastic weather generators generate time series of single climate variables conditioned on prescribed general time series statistics. They are less dependent on GCM skills but can generate physically inconsistent combinations of regional weather variables since they usually generate time series for different variables individually. In general, the application of statistical schemes is confined to projections of similar climates that do not overstrain the stationarity assumption implicit in statistical schemes. This explains their frequent application in regional climate impact studies since these typically deal with near-future climate projections only.

Here we use a resampling approach based on weather analogs. Our statistical analog resampling (STAR) scheme generates ensembles of daily time series that optimally fit a prescribed linear temperature trend (mean and long-term linear increase; see Orlowsky et al. 2008). This temperature trend is the only constraint for the resampling, which is why STAR is located somewhere in between classical downscaling techniques and stand-alone climate modeling approaches. Thus, we try to combine the advantages of the analog approaches (consistency between different variables) and the weather generators (independence on GCM simulations). From the ensemble projections, future climate statistics such as long-term averages or extreme events are estimated. Since these projections are obtained by resampling from past observations, STAR can be seen as an extended bootstrap approach (Efron and Tibshirani 1993) in which the resampling is conditioned on the prescribed temperature trend.

For demonstration purposes, we select the Yangtze River basin in central China. The climate of this region is complex and includes temperate inland, plateau, and monsoonal climatic regions. They are all transected by the Yangtze River, which provides a natural cross section through central China. Since it is one of the most important waterways of the world, reliable projections of its future climate are an important challenge.

In the following, section 2 introduces our bootstrap extension—the statistical analog resampling scheme. Observational and GCM data are described in section 3, together with a cross-validation experiment that demonstrates the applicability of our bootstrapping to the Yangtze River basin. Section 4 analyzes the observed present-day climate (training period 1961–2000) along the Yangtze River at single stations and the adjacent future projections (2001–40). Both the training period climate and the future projections are compared with GCM simulations. Section 5 draws some conclusions on the applicability of STAR for future regional climate projections.

2. Bootstrapping for climate projections

Estimating distributions of sample parameters (e.g., confidence intervals for sample mean, return periods, etc.) by resampling—"bootstrapping"—from a given sample or time series (Efron 1979; 1981) has become a standard approach. Bootstrapping involves time-consuming computations and is therefore intended for situations where distributions cannot be derived from theoretical considerations (Efron and Tibshirani 1993). In climate science, bootstrapping has been used, for example, to estimate the uncertainty of flood return levels (Mudelsee et al. 2003; Rust et al. 2010) and of statistically downscaled meteorological variables (Dibike et al. 2008).

Here we want to obtain ensembles of future climate projections by bootstrapping from a training period sample of past daily observations. Typically, the future climate is expected to be warmer than the training period climate. Since the warming in observations and GCM simulations is one of the most robust climate signals, and to reduce the dependency on single GCM runs, our bootstrap ensemble shall be constrained by a prescribed

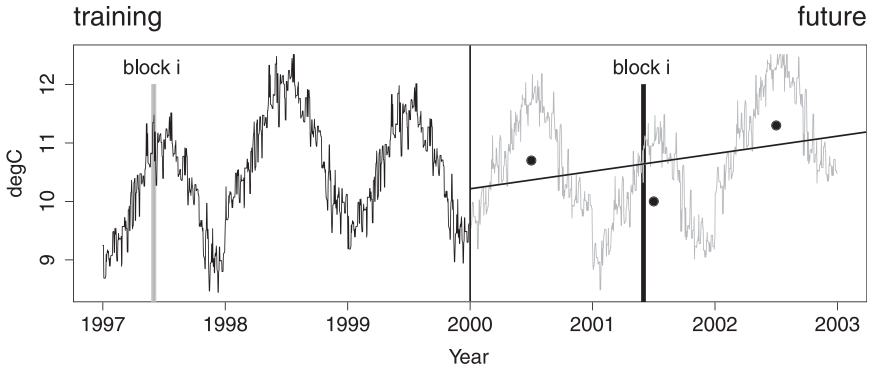

FIG. 1. Bootstrapping 12-day blocks of a training period temperature series (black) for future temperature series (gray), constrained by a prescribed future temperature trend (black line) w.r.t. the annual means (black dots). Temperatures of a suitable block *i* from the training period and the associated calendar dates (taking all weather observations of block *i* with them) are assigned to a block in the future period, conditioned on the temperatures of block *i*. In this illustrative example, the 12 future days starting at 29 Apr 2001 are mapped onto the 12 days starting at 26 Apr 1997.

temperature trend (average and long-term linear increase) only. For reference, Fig. 2a shows that the linear trend in our case gives a good approximation to the temperature evolution.

If we were interested in temperature alone, the "intentionally biased bootstrap" (Hall and Presnell 1999b) would be useful, where the probabilities for the resampling are adapted to given constraints. For example, if a sample of daily temperature observations was to be drawn from the training period sample, with a warmer average than the training period average, the intentionally biased bootstrap would preferably select warm temperature observations (Hall and Presnell 1999a). However, since we are interested not only in the future temperature average but in any kind of climate statistics (variability, annual cycles, extremes, persistence, etc.) for any climate variable, the formulation of all such constraints in the context of an intentionally biased bootstrap (Davison and Hinkley 1997) is not straightforward. Therefore, instead of directly prescribing probabilities for the resampling of the training period observations like in the intentionally biased bootstrap, we bootstrap according to a set of heuristic rules. This set ensures that the bootstrapped series comply with the prescribed trend and, in addition, are physically realistic. This, like in the intentionally biased bootstrap, results in adapted probabilities for the resampling, which, in our case, are defined indirectly by the set of heuristic rules.

a. Bootstrapped weather ensembles conditioned on a future temperature trend

Since our only constraint is a temperature trend, we start with a bootstrap ensemble of daily temperature observations resampled from the training period. A set of heuristic rules for the resampling ensures that the ensemble members reproduce the prescribed temperature trend and realistic annual cycles (see Fig. 1). Inspired by the moving block bootstrap (Efron and Tibshirani 1993; Lahiri 2003), we bootstrap blocks of temperature observations (of 12-day length) rather than single-day observations (e.g., Werner and Gerstengarbe 1997). Experiments with different block lengths suggest that 12-day blocks yield bootstrap series with realistic persistence behavior (physically associated with large-scale circulation patterns).

Since the bootstrapped temperature observations belong to dates from the training period, the temperature series ensemble can be extended to a bootstrap ensemble of calendar dates (assume a single-station setting for now, for regional projections see below). Each ensemble member therefore consists of a date-to-date-mapping,

$$f\text{: future period} \rightarrow \text{training period},$$

assigning each date of the future period to a date (and its concurrent weather observations) from the training period, which may be selected more than once. A future temperature series generated by applying f reproduces the prescribed temperature trend, which means that

$$\text{linear regression}\,[(T_{f(t)}), t \leftarrow \text{future period}] = \text{prescribed trend}$$

holds within a chosen tolerance, which, for this paper, is set to 0.25 K. Note that trends other than linear ones are feasible, although this may lead to convergence problems. For details about how f is constructed, refer to Orlowsky et al. (2008).

By applying f, future series for any kind of observations available at the dates of the training period can be obtained, for example, station observations, monsoon indices, and river runoff and typhoon occurrences. Thus conserving past weather information in the future bootstrap series is equivalent to the analog approaches.

For regional multistation projections, a preparatory step identifies climatological subregions by a hierarchical cluster analysis based on temperature and precipitation. Individual temperature trends are prescribed to one representative station of each subregion. This reduces the complexity and allows for the representation of spatial patterns of future climate variables in the constraints. Here, five subregions and representative stations are identified (see Fig. 3). Note that, besides determining the representative stations and their trends, no adaptation or calibration specific to the region of interest is necessary.

b. *Properties of the bootstrapped weather ensembles*

The bootstrap/analog approach ensures that at each time step spatial fields and combinations of variables are physically consistent since they were once concurrent real-world observations (no trend elimination or any other alteration is applied prior to resampling).

Owing to its design, our approach produces conservative projections in the sense that, if the prescribed future trend continues the training period trend, any systematic change in the set of observables linked to the temperature trend of the training period will continue in the future period. For example, if during the training period a warming is observed and for the future a further warming is prescribed, then any trends linked to the observed warming will be likely to continue in the future projections. This agrees with the intuition that, on the near-future time scale (which we are dealing with here), changes of the physical and statistical relationships within the climate system are small.

Bootstrapping schemes in general tend to reduce variability and persistence. Although sometimes detectable, these effects are weak in STAR projections [see the case study in Orlowsky et al. (2008)].

STAR is implicitly based on the important assumption that joint statistical properties of the different meteorological observables are the same in the training and the future period. This is almost certainly not the case for a changing climate and, in particular, not for the end of the future period with the strongest warming. However, cross-validations as in Orlowsky et al. (2008) or in this study show that the errors resulting from this shortcoming are acceptable, at least for the long-term climatological statistics examined here.

To generate climates with warmer average temperatures than in the training period, STAR has to preferably select warm blocks (like the intentionally biased bootstrap would do), in particular for the end of the future period (with the most elevated temperatures), which can reduce the size of the sample of blocks considerably. This effect is shown for one representative station (Fig. 2b), displaying frequencies at which temperatures are selected from the training period as a function of the future year. It is obvious that the use of high summer temperatures becomes more and more frequent and that low temperatures are used less by the end of the future period. The bandwidth and the size of the sample from which blocks can be chosen at the end of the future period is thus narrowed. This leads to a decrease of the amplitude of the annual cycle and to a reduced variability at the end of the future period.

Obviously, this limits the applicability of such schemes to projections of future climates that are ''within the variability of the training period.'' This condition can be evaluated a posteriori by an ''internal variability conservation'' criterion (see Orlowsky et al. 2008): The variability of a training sample is large enough to bootstrap series with a given future temperature trend if the temperature anomalies (i.e., the time series after removing long-term trend and annual cycle) of the training series and a future bootstrapped series can be seen as originating from the same distribution. In this case the imposed trend does not lead to a statistically visible reduction of variability. Experiments with different prescribed trends suggest that according to this criterion the warming in the training period can continue to the future period with the same strength (i.e., if a warming of 1 K has been observed, a further warming of 1 K is feasible). However, from our experience, even larger prescribed future trends can yield satisfactory results, particularly compared to the performance of dynamical models (Orlowsky et al. 2008), if long-term statistics are considered, for which a reduced variability, especially at the end of the future period, is less important.

3. Data and validation

STAR resamples observational station data to generate ensembles of future climate projections, which are constrained by a linear temperature trend. For the future projections (from 2001 to 2040) of this paper, the trend is derived from a GCM scenario run (ECHAM5). Both observational and GCM data are described (section 3a). A cross-validation experiment that studies the applicability of STAR for the Yangtze River basin is presented in section 3b.

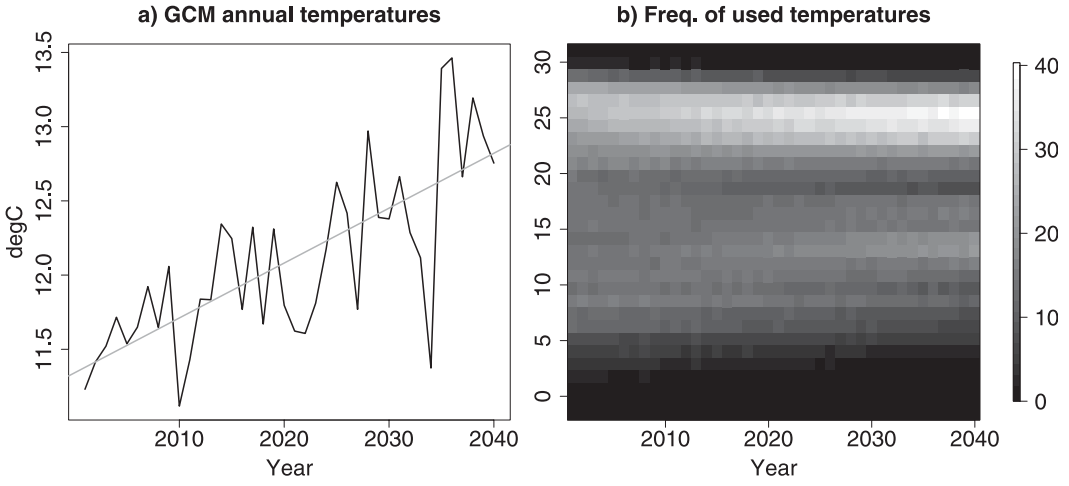

FIG. 2. (a) ECHAM5 annual temperatures, averaged over the five grid cells containing the representative stations (see Fig. 3a), illustrating the linearity of the temperature increase (the variance explained by the linear fit is 53%). (b) Frequencies per future calendar year (grayscale coded) of the bootstrapped temperatures from the representative station in the middle (Fig. 3a), averaged over the entire ensemble.

a. Data

1) OBSERVATIONAL DATA

Daily time series of the following variables are analyzed for the present day (training) and subsequent future climate projection: temperature, precipitation, Yangtze runoff, a monsoon index, and typhoons in the East China Sea.

(i) Temperature and precipitation are taken from Feng et al. (2004). The variables are daily minimum, mean and maximum temperature, and precipitation. We use 172 stations along the Yangtze (Fig. 3), where we have uninterrupted temperature and precipitation time series available from 1961 to 2000. Since the training dataset ends in 2000, the years from 2001 to 2040 are chosen as the future period. Station density varies across China, with fewer stations per area in the mountainous regions compared to the eastern plains (see Fig. 3).

(ii) Runoff at the stations Cuntan (29°37′N, 106°36′E; 165 m MSL) and Datong (30°46′N, 117°37′E; 9 m MSL) along the Yangtze supplements the information about the water cycle (see Wang et al. 2008).

(iii) Monsoon index: The Western North Pacific Monsoon Index (WNPMI; see Wang et al. 2001; daily data from 1961 to 2000 available from the Meteorological Department of the University of Hawaii at Manoa) is chosen as it captures the circulation affecting inland rainfall in the Yangtze River catchment. It is defined by the horizontal gradient of lower tropospheric (850 hPa) zonal wind, which characterizes the intensity of the North Pacific subtropical high by its vorticity [WNPMI = $U_{850}(1)$ minus $U_{850}(2)$, averaged over two rectangular areas (1) and (2); Fig. 3].

(iv) Typhoons: Tropical cyclone track data in the rectangular area (20°–35°N, 115°–130°E; see Fig. 3) provide information about typhoon occurrence and intensity (date, position, and wind speed). The dataset is available from the Joint Typhoon Warning Center (available online at http://www.usno.navy.mil/JTWC; compiled by F. Sielmann 2009, personal communication). To study the typhoons with landfall, we further analyze the tropical cyclone tracks that reach over land in the rectangular area. For this, the coast is approximated by the polygon (22°N, 116°E; 30°N, 123°E; 35°N, 120°E), and the region to its west is considered as land.

2) MODEL DATA

Data from the GCM ECHAM5 (Roeckner et al. 2003), which, compared to other GCMs, performs relatively well over China (Xu et al. 2007), are used twofold here.

(i) They are compared both with observations from the training period and with future projections. Therefore, an ECHAM5 run covering the training period 1961–2000 (Roeckner et al. 2008a) is analyzed jointly with an ECHAM5 simulation for the future period 2001–40 (Roeckner et al. 2008b), which is driven by the Special Report on Emissions Scenarios SRES-A1B scenario (Nakicenovic and Swart 2000). Both runs come on a Gaussian grid with a resolution of

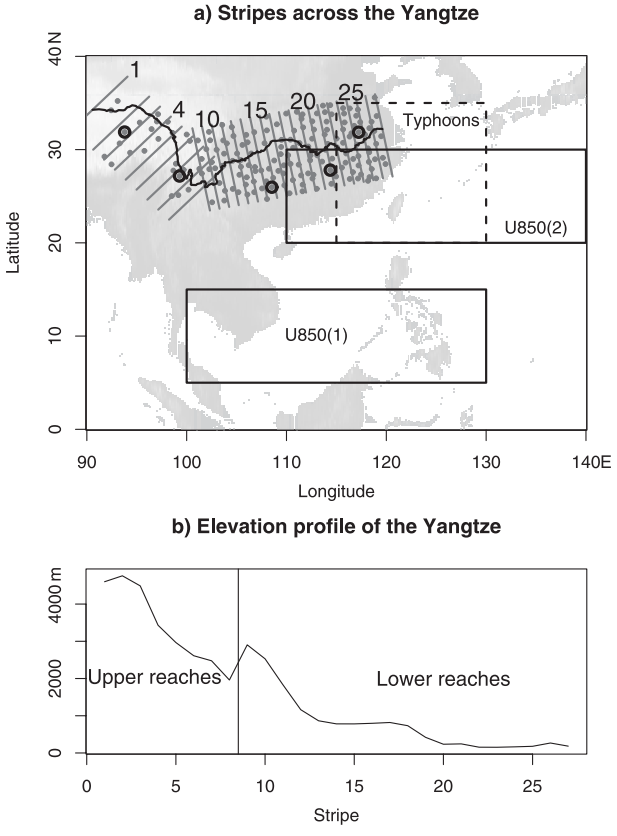

FIG. 3. (a) Stations of the Yangtze River catchment (gray points), Yangtze River (black), and stripes by which the station data is grouped (gray parallel lines); topography (grayscale coded, the Tibetan Plateau in white), representative stations (cluster centroids) for the bootstrapped future projections (black circles), areas for calculating the WNPMI (solid rectangles), and for analyzing typhoons (dashed rectangle). (b) The elevation profile along the Yangtze represents an average altitude of the stripes; the vertical line marks the boundary between upper and lower reaches of the Yangtze River.

approximately 1.875°. The twentieth-century run is forced by observed greenhouse gas concentrations; the last year (2000) serves to initialize the subsequent A1B run for the twenty-first-century scenario. Hence, both ECHAM5 simulations represent a continuous climate evolution from 1961 to 2040.

(ii) The temperature trend, which is prescribed for the future projections, is determined from the ECHAM5–A1B run: The linear temperature increases of the annual mean temperatures from 2001 to 2040 are calculated for the grid cells that embed the representative stations. They range from 0.7 to 1.7 K. These increases are much stronger than the ones observed in the training period (ranging between 0.1 and 0.9 K) and are thus likely to yield climates lying outside the training period variability (cf. section 2b). Further, note that in GCM simulations, temperature averages often deviate from observations, while temperature changes are more realistic. The GCM-simulated increases of temperature from 2001 to 2040 are therefore assumed to start from the temperature levels observed at the representative stations, instead of the respective GCM-simulated temperature levels, of the year 2000. Underlying this procedure is the assumption that the temperature bias of the GCM is time independent, which could be problematic since GCMs are known to have drifts. However, these drifts are of a smaller order of magnitude over our 40-yr period than the bias itself and should, therefore, not compromise our results.

b. Validation

The performance of STAR in the Yangtze River catchment is evaluated in a cross-validation experiment that supplements a model cross-validation for the North Atlantic European sector (Orlowsky and Fraedrich 2009). It is set up to generate the climate of a validation period (from 1981 to 2000) from the independent preceding time span 1961 to 1980. The same five representative stations are used as for the future projections (Fig. 3). The prescribed linear temperature trend for the validation period is determined by a regression analysis of the annual mean temperature series at the five representative stations from 1981 to 2000; 100 ensemble members are created. Generally, these projections do not fulfill the a posteriori variability conservation criterion from section 2b, which means that the climate of the validation period lies outside of the training period variability. A successful cross-validation in spite of this demanding setting gives strong evidence of the robustness of the projections, at least for the long-term statistics considered here. The comparison of the ''true'' (observed) validation climate with the STAR projections shows the following results (Table 1):

(i) The agreement between validation period observations and projections is close for all statistics analyzed: annual mean temperature and precipitation, monsoon/precipitation correlation, lengths of dry spells, 90% quantile of Yangtze runoffs as flood indicators, average summer [June–August (JJA)] monsoon strength, and annual occurrences of typhoons.

(ii) The spread of the ensemble is narrow and always includes the observed validation period statistics. This hints at the robustness of the results, despite the short length of 20 yr of the projected time series. Note that in a similar cross-validation for the Elbe River catchment (Orlowsky et al. 2008), the ensemble spread is larger for several statistics, showing that the narrow spread found here is not a methodological artifact.

These results suggest that STAR is a suitable tool for future climate projections of the Yangtze River catchment,

TABLE 1. STAR validation: Observations (Obs) and projections, both for the validation period from 1981 to 2000. For both upper and lower reaches (see Fig. 3 and section 4 for their definition): mean annual temperature and precipitation, monsoon/precipitation correlation, mean dry spells, and Yangtze runoffs (the Cuntan and Datong gauges for the upper and lower reach, respectively). Concerning the adjacent Pacific: summer monsoon, measured by the average JJA WNPMI, and typhoon days yr^{-1} (see Fig. 3). Both ensemble average and ensemble spread (in parentheses) are given.

	Upper reach		Lower reach	
Validation Period 1981–2000	Obs	STAR	Obs	STAR
Mean temperature (°C)	5.85	5.88 (5.84 to 5.95)	15.55	15.55 (15.49 to 15.60)
Annual precipitation (mm yr^{-1})	712	696 (680 to 714)	1204	1199 (1168 to 1243)
Correlation monsoon/precipitation	0.00	−0.03 (−0.06 to 0.01)	−0.11	−0.09 (−0.11 to −0.04)
Mean dry spell (days)	5.65	5.97 (5.54 to 6.38)	3.36	3.25 (3.04 to 3.42)
90% quantile runoff (m^3 s^{-1})	24 300	24 517 (23 700 to 25 400)	50 100	49 403 (47 900 to 51 060)
Monsoon (JJA)			4.24	4.97 (4.12 to 5.63)
Annual typhoon days yr^{-1}			33.25	33.70 (30.60 to 35.80)

despite the variability conservation criterion (section 2b) not being fully satisfied.

4. Application to the Yangtze: Present and future climates

The Yangtze River runs approximately 6300 km from its origins in the eastern Tibetan Plateau at 4000 m to the East China Sea. It transects different climate types—such as plateau, temperate inland, and monsoonal climates—which are controlled by (i) topography, (ii) latitude characterizing radiative forcing and seasonality, and (iii) monsoonal systems induced by the land–sea contrast [e.g., Domrös and Peng (1988); for comparison, see the moisture-based climate classification (Wu et al. 2006) or the widely used Köppen classification (Fraedrich et al. 2001)]. This climatological complexity is challenging for statistical climate projections.

The present-day and future Yangtze climates are analyzed in ECHAM5 simulations and in station observations/future projections. For ECHAM5, the grid cells covering the upper reaches (i.e., 23°–37°N, 90°–102°E) and those covering the lower reaches (25°–35°N, 101°–120°E) are averaged. For the analysis of the observations and bootstrap projections, the course of the Yangtze is approximated by two straight lines (see Fig. 3a): one characterizes the upper reaches ranging from the sources in the high elevations to the eastern part of the Tibetan Plateau (above ~2000 m); the other line describes the lower reaches continuing eastward. The two lines cross approximately at the main bend of the Yangtze River near Panzhihua. Upper (lower) reaches are represented by 8 (19) stripes perpendicular to the two lines; station data within each stripe is averaged, leading to a single time series of daily meteorological observations per stripe; the double width of the first stripe is due to station scarcity. Climate statistics of these averaged time series are presented as profiles (see Fig. 3b, where upper and lower reaches are separated by a vertical line).

The future bootstrap ensemble contains 100 projections. None of these comply with the a posteriori variability conservation criterion from section 2b. Strictly speaking, the climatological variability of the training period is, therefore, overstretched by the ECHAM5-derived temperature trends. However, since our analysis is restricted to long-term statistics and because of the encouraging cross-validation experiment (which also does not satisfy the a posteriori variability conservation criterion from section 2b), we assume that the results presented now are not critically affected by this drawback. Before the future projections along the Yangtze are discussed in detail, the averages of the upper and lower reaches are summarized (Table 2).

(i) The GCM simulation by ECHAM5 for the present-day period (1961–2000) and the future A1B scenario (2001–40) show an overall temperature increase of about 0.7 K (the weighted average of upper and lower reaches); the increase is larger in the upper reaches of the Yangtze. Note that STAR projects a higher temperature increase from training to future period than ECHAM5. This is because the prescribed temperature increase is taken from ECHAM5, but the prescribed average is based on the training period observations (see section 3a), which leads to different increases of the average temperatures

TABLE 2. Annual means of (a) temperature (°C), (b) annual precipitation (mm yr^{-1}), and (c) monsoon/precipitation correlation: Upper and lower Yangtze reaches during training (1961–2000) and future (2001–40) period based on observations, STAR projections, and climate model simulations (ECHAM5). The results of the future period are given as entire-ensemble averages and, in parentheses, as spread of the ensemble.

	Upper reach		Lower reach	
Period	Obs/STAR	EH5	Obs/STAR	EH5
(a) Temperature				
1961–2000	5.71	5.12	15.49	14.19
2001–40	6.87 (6.80 to 6.93)	6.07	16.30 (16.24 to 16.35)	14.75
(b) Precipitation				
1961–2000	698.46	1576.81	1198.52	1374.99
2001–40	767.56 (747.21 to 796.95)	1576.55	1307.70 (1264.78 to 1346.89)	1386.35
(c) Correlation monsoon/precipitation				
1961–2000	−0.01	−0.08	−0.09	−0.05
2001–40	−0.04 (−0.07 to −0.01)	−0.05	−0.16 (−0.19 to −0.14)	−0.06

from the training to the future period in observations/STAR and ECHAM5, respectively.

(ii) The bootstrap ensemble indicates a precipitation increase that is more pronounced in the lower reaches. Climate model precipitation (ECHAM5, simulated for the training period) is much higher than observed, and its spatial distribution does not coincide with station data: the upper reaches in the observations are significantly drier than the lower reaches, whereas ECHAM5 data indicate slightly wetter upper reaches. This mismatch is supported by Hagemann et al. (2006), who note that Yangtze River catchment precipitation is overestimated by ECHAM5 due to excessive monsoon precipitation, reaching from the southern slopes of the Himalayas into the Yangtze River basin. Thus, ECHAM5 precipitation does not serve as a good reference in this region. Another GCM (Gao et al. 2006) shows exaggerated precipitation east of the Tibetan Plateau, at least in part because of the too-coarse horizontal resolution (see also Gao et al. 2001).

(iii) The influence of the daily monsoon (WNPMI) on precipitation is measured by a rank-based correlation coefficient. Significant correlations exist only in the lower reaches (see Fig. 6 and the monsoon paragraph in section 2b), which become stronger in the future ensemble, whereas correlations in ECHAM5 hardly change. For the training period, ECHAM5 overestimates the correlation strength in the upper reaches.

a. Temperature and precipitation: Annual cycles and profiles

The future temperature and precipitation climates (2001–40) are compared with the training period (1961–2000): First, the annual cycles averaged over the upper and lower reaches are shown (Figs. 4a and 4b), with annual cycles of Yangtze runoffs completing the water cycle information (Fig. 4c). Second, the annual mean profiles of temperature and precipitation following the Yangtze (Figs. 5a and 5b) are analyzed.

1) ANNUAL CYCLES

The bootstrapped *future annual temperature cycle* averaged over upper and lower Yangtze reaches (Fig. 4a) shows warming in winter, spring, and autumn, while the summer season experiences a moderate cooling. The summer cooling is weaker in the upper reaches, where the ensemble spread of the future summer temperature (i.e., the range of all summer temperatures from the bootstrap ensemble) shows an overlap with the training period. The lower reaches show a stronger summer cooling. This coincides with the projected 90% quantile of daily maximum temperatures in the lower Yangtze reaches (not shown), which also decreases. This summer cooling has already been observed at the end of the past century (1971–2000; Wu et al. 2006).

The bootstrapped *future annual precipitation cycle* (Fig. 4b) of upper and lower reaches precipitation shows an increase in summer. This coincides with the projected cooling from June to August. The summer monsoon season is extended to autumn in both upper and, even more pronounced, lower reaches; in the upper reaches the premonsoon rainfall also increases. The observed decrease of the rainfall amount in spring and autumn (from 1971 to 2000), Wu et al. (2006) is not continued in the future ensembles. The differences between the training and the future periods are stronger for the summer months (compared to the winter months), and the strongest differences occur in the lower reaches; if relative differences are considered, the upper reaches reveal the strongest increase in late fall/winter, while the lower reaches show increases mainly in late summer and autumn. This agrees with the observation that rainfall variability is greater in summer than in winter and that this difference is more pronounced for the eastern parts of China (Domrös and Peng 1988).

The bootstrapped *future annual runoff cycle* (Fig. 4c) corresponds to the one of precipitation: For example, in the upper reaches April and May precipitation increases in the future. This increase is also found in the spring runoff of the upper reaches and, consequently, in the spring runoff of the lower reaches. The lower reach precipitation has its most pronounced rise in August and

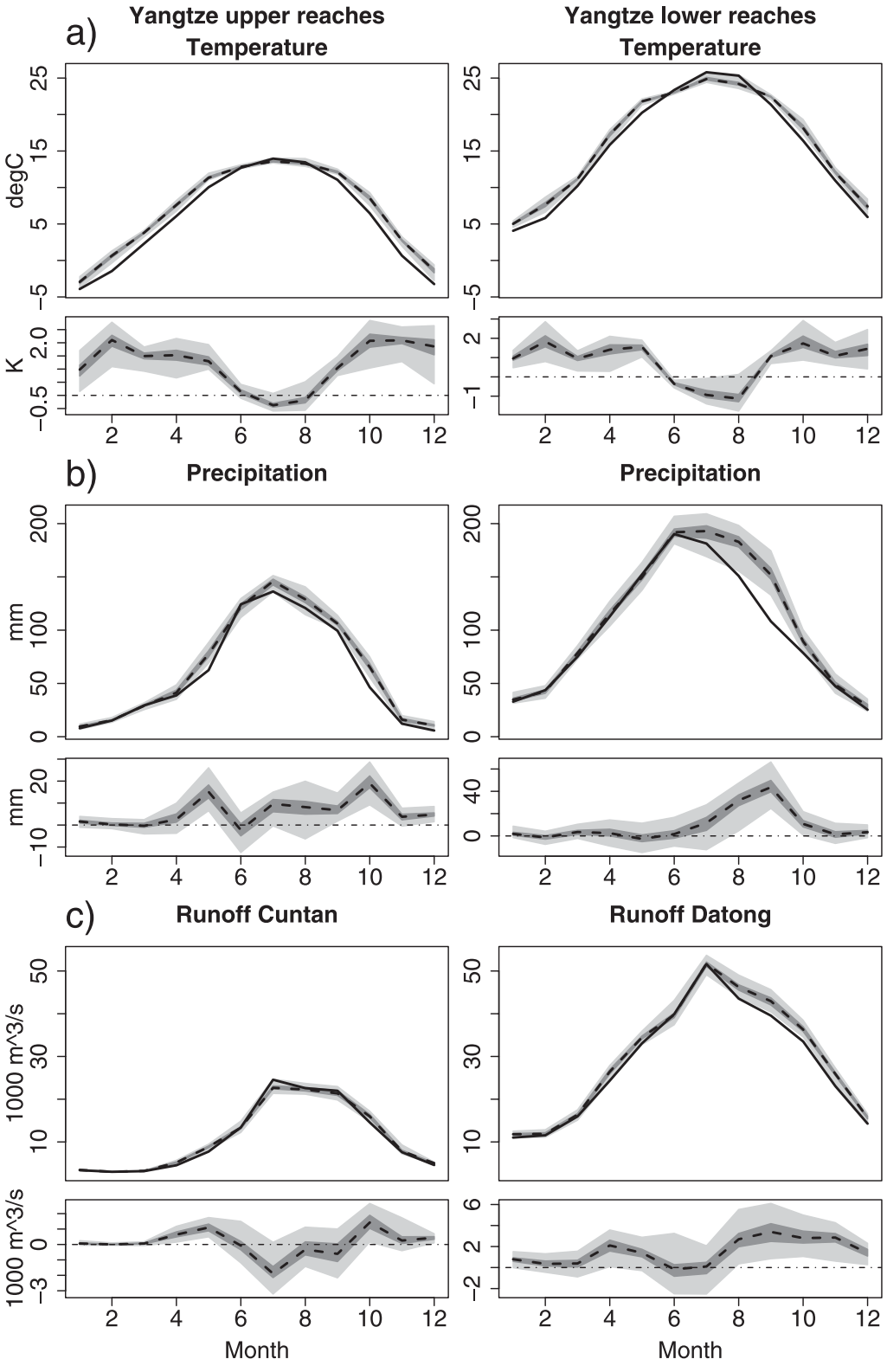

FIG. 4. (top) Annual cycles (monthly means/sums) of (a) temperature, (b) precipitation, and (c) runoff (at Cuntan and Datong) for the (left) upper and (right) lower reach of the Yangtze: annual cycles from the observed station data 1961–2000 (full line); spread (light gray shading), interquartile range (dark gray shading), and median (dashed black line) of the STAR ensemble projections (2001–40). (bottom) Differences of future projections minus training period observations, shading and lines as in the top panels.

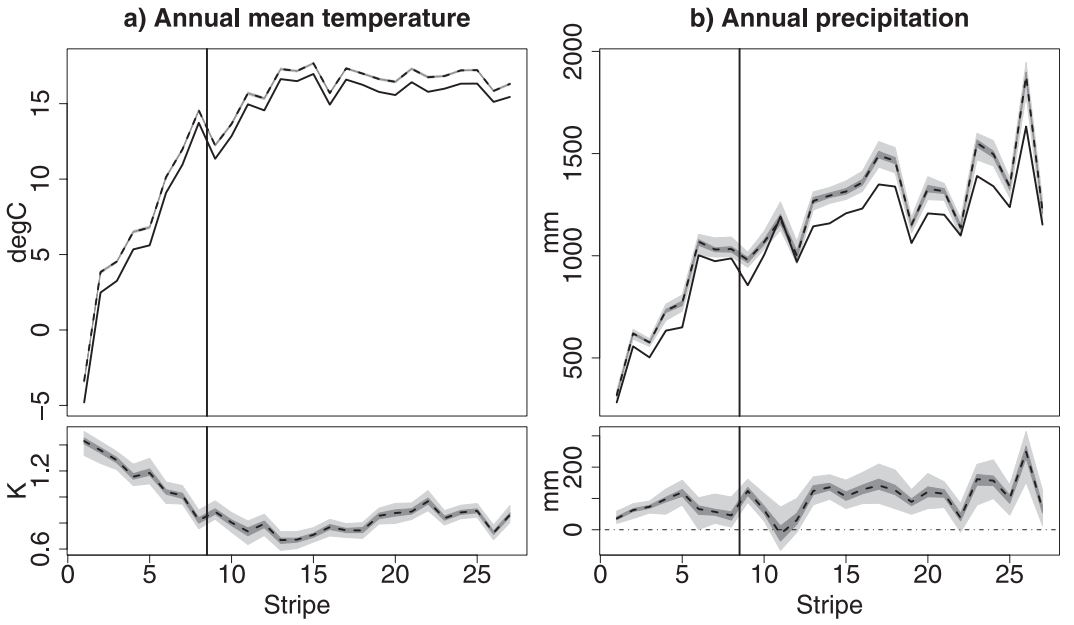

FIG. 5. (top) Annual mean (a) temperature and (b) precipitation along the Yangtze: profiles from the observed station data 1961–2000 (solid black line); spread (light gray shading), interquartile range (dark grayshading), and median (dashed black line) of the STAR ensemble projections (2001–40). Averages are taken on stripes perpendicular to the two Yangtze River segments (see Fig. 3, upper and lower reaches are separated by a vertical line). The stripes are numbered along the *x* axis. (bottom) Differences of future projections minus training period observations; shades and lines as in the top panel.

September, thus increasing autumn and early winter runoff in the lower reaches.

Comparing these observations and future projections to climate model simulations, the following is noted: (i) The future (2001–40) annual temperature cycle in ECHAM5 is not the same as in the STAR projections (not shown). Although winter and spring experience a slightly stronger warming than the rest of the year in the ECHAM5 data, the summer cooling from the bootstrap ensemble is not found. (ii) Analyzing East Asian summer monsoon under climate change [for the twenty-first century, see Kripalani et al. (2007)] reveals that many GCMs extend the summer monsoon season into spring and autumn, together with an overall increase of monsoon precipitation. The bootstrap projections are in agreement with this finding. However, neither the GCMs studied in Kripalani et al. (2007) nor the ECHAM5 data used here show the asymmetry of the extension toward the autumn months projected by STAR.

2) PROFILES

The *profile of average temperature* shows a clear dependence on topography, decreasing with increasing elevation (see Fig. 5a). The future projections span a very narrow band of warmer temperatures according to the prescribed temperature trend. Temperature increase is most pronounced for the upper reaches of the Yangtze River basin.

The *profile of annual precipitation* also corresponds to the inverted elevation profile (see Fig. 5b). The future ensemble indicates higher annual mean precipitation, with particularly pronounced increases in the lower reaches where precipitation is also highest. Note that observations (from 1971 to 2000, Wu et al. 2006) reveal a detectable positive trend in precipitation for most of the Yangtze. The only parts that show negative trends (although statistically not significant) are the source region and stripes 10–13. In these parts, STAR projects only very small changes, whereas the other parts see a continuation of the precipitation increases from the training period. Also for annual precipitation, the range of the ensemble is narrow, which hints at a robust projection. The 90% quantile of daily precipitation increases in the future ensemble, corresponding to episodes of higher precipitation in the future (not shown).

As a note, we add that these future trends do not lead to changing climate classes according to the Köppen classification (Fraedrich et al. 2001, not shown).

b. Climate impacts and extremes

Central China and especially the Yangtze are regularly affected by droughts and floods. Near the end of the training period (1961–2000), several big flood events occurred with devastating economic and human losses. Typhoons also frequently affect the shore of the China

Sea. This section analyzes the future STAR projections with respect to some climate phenomena that have impacts on society, namely, heat and cold waves, droughts/dryness, floods, monsoons, and typhoons.

1) HEAT WAVES, FROST, AND DRY SPELLS

Heat waves (average period lengths of consecutive days with $T_{max} \geq 25$°C) at the Yangtze estuary (stripes 20–27) increase from about 13.7 days (training) to 15.6 (ensemble mean, ensemble spread: 13.6–17.9 days), while there is only little change in stripes 1–19 (not shown). On the other hand, cold waves (average period lengths of days with $T_{min} \leq 0$°C) decrease, in the averaged upper reaches from 15.4 days (training) to 13.1 (ensemble mean, ensemble spread: 12.5–14.1 days) and in the lower reaches from 3.5 days (training) to 3.0 (ensemble mean, ensemble spread: 2.7–3.2 days).

In STAR projections, persistence statistics can differ from those of the training period. Here, ''warm'' blocks are preferably selected for the prescribed warming, which leads to increasing heat wave lengths and decreasing cold wave lengths.

Dry spells (average period lengths of consecutive days without precipitation) follow the elevation profile, with lengths of more than six days in the Tibetan plateau and less than four days in the eastern lower plains (see Fig. 6a). Consistent with the increasing precipitation, averages of the projected dry spells decrease (compared to present-day climate) strongest in the upper reaches. The ensemble spread of dry spells is also consistent with the ensemble spread of precipitation (Fig. 5b) and the reduced probability of moderate-to-extreme standardized precipitation index (SPI) dry states (see the next paragraph and Fig. 7b). According to the future projections, dry spells become less relevant in the Yangtze River catchment.

2) WETNESS AND DRYNESS

The SPI (McKee et al. 1993) is introduced to monitor dryness and wetness using precipitation only. Based on an ''equal probability transformation'' (Bordi and Sutera 2001; Bordi et al. 2004), it gives a uniform measure for dryness and wetness in climatically differing regions. The monthly SPI chosen here is representative for the meteorological drought time scale. A gamma distribution is fitted for the precipitation time series of a given calendar month, its cumulation determined, and the SPI appointed following the standard normal distribution by conserving the cumulative probability. Dryness and wetness are then classified as follows: moderate-to-severe wetness (dryness): $1 \leq \text{SPI} < 2$ ($-1 \geq \text{SPI} > -2$); extreme wet (dry) conditions $\text{SPI} \geq 2$ ($\text{SPI} \leq -2$).

Changes of wetness or dryness can be quantified in SPI terms (Sienz et al. 2007) using the same distribution for the present-day training period and the future ensembles. The overall increase in precipitation leads to the following results:

(i) The number of moderate-to-extreme wet classes ($\text{SPI} \geq 1$) increases by about 7.5 percentage points (Fig. 7a) in the lower reaches. Thus, about 35 (out of 40 yr $\times$ 12 = 480 months) more wet months (from moderate to extreme) are expected in the projected future period compared to the training period. This increase is even more pronounced in the upper reaches. Especially, the extreme wet months occur more frequently in the upper reaches (not shown). In contrast, the 90% quantile of daily precipitation (not shown) increases primarily in the lower reaches.

(ii) The number of moderate-to-extreme dry classes ($\text{SPI} \leq -1$, Fig. 7b) decreases by about 3 percentage points (corresponding to 14 dry months less), but the extreme drought events ($\text{SPI} \leq -2$, not shown) hardly change. Thus, the decrease in dry conditions is overbalanced by a significantly larger number of wet events.

3) FLOODS

Ensembles of future daily runoff series are generated by rearranging runoffs from the training period following the STAR date-to-date-mappings. As an indicator for floods, the 90% quantile is computed at the two gauges—Cuntan and Datong—that are representative of the upper and the lower reaches, respectively. For the upper reaches, the future ensemble gives an unchanged 90% quantile: observed training period average of 24 400 $m^3 s^{-1}$, future ensemble average of 24 038 $m^3 s^{-1}$, and future ensemble spread between 23 100 and 24 800 $m^3 s^{-1}$. For the lower reaches, a slight increase is noted: observed training period average of 49 100 $m^3 s^{-1}$, future ensemble average of 51 538 $m^3 s^{-1}$, and future ensemble spread between 49 700 and 54 300 $m^3 s^{-1}$. The higher 90% quantile is in agreement with the larger runoffs in the future period of the lower reaches (Fig. 4c).

4) MONSOON

The Yangtze summer monsoon depends on the summer easterlies emerging from the North Pacific (Wang et al. 2001) and thus on the shape and position of the North Pacific subtropical high (Kripalani et al. 2007), which is represented by WNPMI. The future monsoon index series are obtained adopting the date-to-date-mapping. Table 3 summarizes the monsoon index analysis for the present climate and its future projection.

(i) The annual averages hardly differ between training observations and the future ensemble. However, the future ensemble shows a strong decrease of the

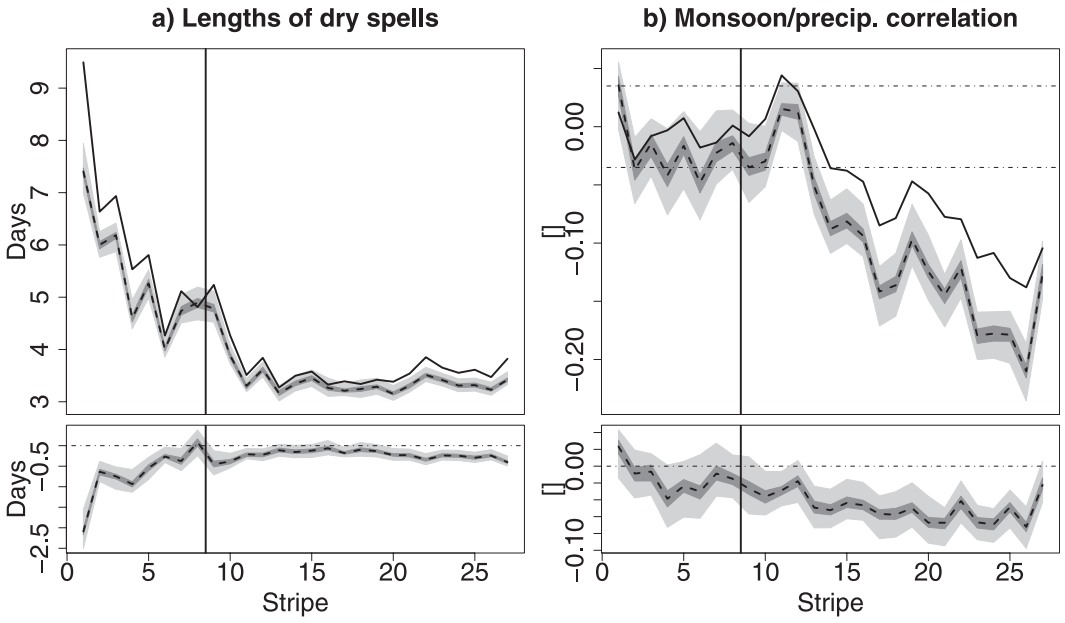

FIG. 6. (top) (a) Average dry spell lengths and (b) correlation between monsoon strength (WNPMI) and daily precipitation along the Yangtze: profiles from the observation period (solid black line); spread (light gray shading), interquartile range (dark gray shading), and median (dashed black line) of the STAR ensemble projections. The dashed–dotted lines in the upper right panel indicate the 90% confidence interval for the null hypothesis (Spearman's $\rho = 0$, serial correlation taken into account). (bottom) Differences of future projections minus training period observations; shading and lines as in the top panel.

WNPMI in summer (JJA), thereby continuing the negative trend observed during the training period (derived from Wang et al. 2001). The mean summer WNPMI in the ECHAM5 simulations remains almost unchanged from the training to the future period. The annual mean, however, decreases. Note that for the training period, the positive annual mean WNPMI of ECHAM5 contrasts the observed negative one.

(ii) The variability, measured by the standard deviation of the annual and the summer averages, decreases in the future ensemble. This, however, might partly be a model artifact since resampling procedures tend to underestimate variabilities. ECHAM5 variability of both the annual and the summer averages increases from training to the future period.

To analyze the influence of the monsoon on precipitation along the Yangtze, a rank-based correlation coefficient (Spearman's ρ) between daily WNPMI and daily rainfall, of which the long-term trend and annual cycle are removed (see Cleveland et al. 1990), is shown in Fig. 6b. It reveals a weak but significant negative correlation at the Yangtze estuary. In the upper reaches, the correlation vanishes. Apparently, the distance from the sea and possibly the barrier of the Tibetan Plateau reduces the influence of the monsoon on precipitation. Despite the low absolute values of the correlation, the decrease of the correlation strength from the estuary to the Himalayas is systematic. The future ensemble indicates a stronger negative correlation, that is, a stronger monsoon control on Yangtze precipitation for the future period.

The ECHAM5 simulations of training and future period do not show this trend in the WNPMI/rainfall correlation. The correlation contrast between upper and lower reaches in the observations and the bootstrap ensemble is not reproduced in the ECHAM5 data either, which may be a consequence of the overestimated upper reach precipitation (see Table 2).

5) TYPHOONS

The frequency of typhoon days in the East China Sea (Fig. 3a) decreases by approximately 25% in the future projections: in the observed training period there is an average of 33.1 typhoon days yr^{-1}, in the future ensemble an average of 25.3, and the ensemble range is between 21.8 and 30.4. This corresponds to a decrease of approximately 3.3 typhoons yr^{-1} for the future period since an average typhoon lasts for about 2.4 days (in this area). For the subset of typhoon days with landfall (see observational data, section 3), a decrease of about 35% is noted: In the observed training period, there is an average of 5.3 typhoon days yr^{-1} in the future ensemble an average

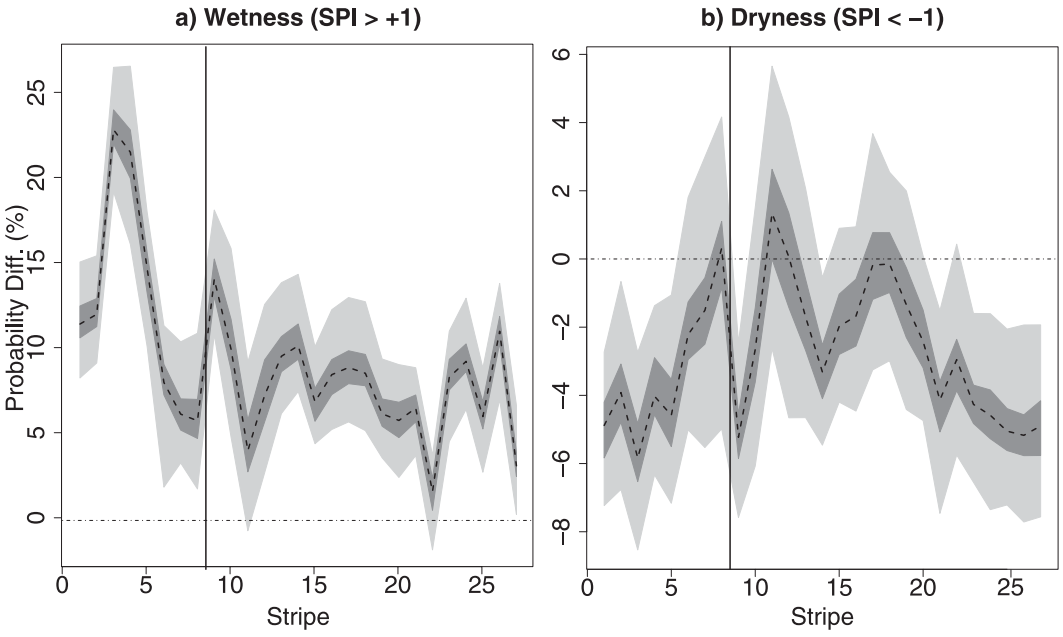

FIG. 7. Changes of moderate-to-extreme (a) wetness and (b) dryness classes of the SPI given as differences (in percentage points) of STAR future projections (2001–40) minus training period observations (1961–2000) along the Yangtze River: spread (light gray shading), interquartile range (dark gray shading), and median (dashed black line) of projected differences. The zero line corresponds to the probability of the training period SPI (16%).

of 3.4, and the ensemble range is between 2.7 and 4.4. Note that a negative trend of the same order of magnitude is observed during the training period (Ho et al. 2004; Chan 2005; Webster et al. 2005), which continues in the future ensemble. This is supported by some GCMs (e.g., ECHAM5), which also simulate a decreasing future typhoon activity in the northwest Pacific (Bengtsson et al. 2007), whereas others simulate unchanging typhoon occurrences (Stowasser et al. 2007).

Many GCM scenarios show more intense typhoons for a future warmer climate (Bengtsson et al. 2007; Stowasser et al. 2007), which is in agreement with an observed intensification of typhoons in the past decades (Webster et al. 2005). The bootstrap projections show this intensification for the typhoons with landfall, but not for the East China Sea in general (Figs. 8a and 8b): Frequencies of all wind speeds decrease by a similar proportion in Fig. 8a. For the landfall typhoons (Fig. 8b), however, the frequencies of lower wind speeds decrease more than the frequencies of higher speeds, which tend to increase. This results in a higher proportion of intense typhoons.

5. Conclusions

A statistical analog resampling (STAR) is employed to obtain future climate profiles along the course of the Yangtze, which transects all of the major climate zones of central China. A validation experiment confirms the applicability of STAR for future Yangtze climate projections. Based on the observed present-day climate along the Yangtze (training period 1961–2000), an ensemble of future climate projections from 2001 to 2040 is generated, constrained by a linear temperature trend that, in our case, is taken from a GCM scenario simulation (ECHAM5). The future climate projections are compared with ECHAM5 simulations for both training and future periods. The following results are noted.

(i) Temperature shows a significant increase that is especially noticeable in the upper reaches of the Yangtze River and in the winter half-year. In summer, the projected temperature is reduced. This summer cooling may be related to enhanced precipitation.

TABLE 3. The monsoon index WNPMI of the training and the future period in observations (Obs), STAR projections (ensemble average and spread), and ECHAM5 simulations (m s^{-1}). (a) Annual means and summer (JJA) means and (b) the respective standard deviations (std dev) are shown.

Period	Obs/STAR	EH5	Obs/STAR	EH5
	Annual mean		JJA mean	
1961–2000	−1.71	1.04	4.49	8.99
2001–40	−1.79	0.79	2.44	8.96
	(−2.04 to −1.43)		(1.93 to 3.48)	
	Interannual std dev		JJA std dev	
1961–2000	0.82	0.95	1.85	2.54
2001–40	0.72	1.16	1.73	2.78
	(0.43 to 0.90)		(1.30 to 2.12)	

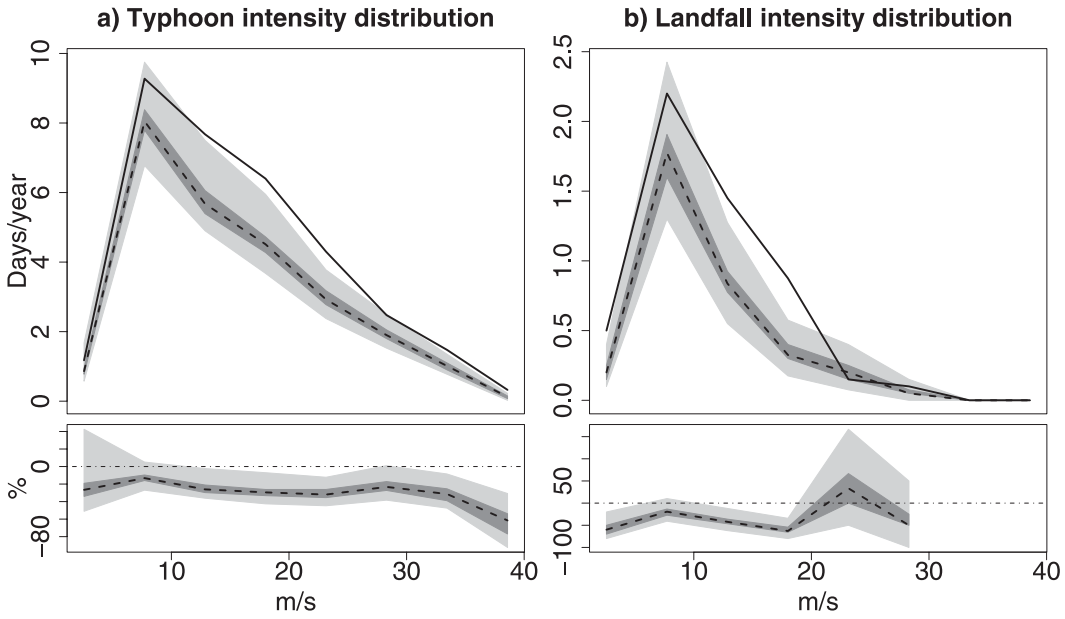

FIG. 8. (a) Frequency distribution (typhoon days yr^{-1}) of typhoon intensity wind speed (m s^{-1}) in the East China Sea and (b) frequency distribution of the typhoon days with landfall. (top) Distribution from the observation period 1961–2000 (solid black line); spread (light gray shading), interquartile range (dark gray shading), and median (dashed black line) of the STAR ensemble projections (2001–40). (bottom) Relative differences of future projections minus training period distribution.

(ii) Precipitation increases in the future projections, occurring particularly in summer and autumn; it is notable along the entire Yangtze profile with a more pronounced increase closer to the estuary. This corresponds to the projected summer cooling, which is physically plausible because of enhanced evaporation. It is supported by an increase (decrease) of SPI wetness (dryness) and decreasing lengths of dry spells. The overall precipitation increase is partly due to an extension of the summer monsoon, which especially in the lower reaches is prolonged into autumn. For comparison, ECHAM5 precipitation shows hardly any change.

(iii) Monsoon: Summer (JJA) averages of the Western North Pacific Monsoon Index (WNPMI) decrease in the future projections. Furthermore, a stronger negative correlation between the WNPMI and precipitation in the lower reaches—that is, a stronger monsoon control on the Yangtze basin precipitation—is found in the future bootstrap ensemble; ECHAM5 simulates an almost unchanging WNPMI.

(iv) The annual runoff cycles of Yangtze stations follow precipitation. The projected 90% quantile, which is a measure for floods, increases slightly in the lower reaches.

(v) Typhoon occurrence decreases by 25% in the future projections, in agreement with several GCM studies. Intensification of typhoons is found in GCM scenarios and in the ensemble of typhoons with landfall.

(vi) Many trends in the projections continue the trends already present in the training period, which supports the plausibility of STAR.

(vii) Profiles along the Yangtze from observations and projections are remarkably ''parallel.'' This is because, at every station, the projected future series are assembled from observations at that very station, thus taking all local characteristics like topography into account. The spatial structure of the climate is therefore highly detailed in the projections and is also meteorologically consistent. Owing to their coarse spatial resolution, GCMs cannot provide this detailed representation of local conditions. This accounts, for example, for the misrepresentation of the annual precipitation contrast between the upper and lower reaches of the Yangtze River in ECHAM5, which overestimates the upper reach precipitation. The missing WNPMI/precipitation correlation contrast between upper and lower reaches in the ECHAM5 simulations may be another consequence.

The systematic errors in GCM simulations of regional climates and their computational costs (compared to STAR: the 100 × 40 yr projections analyzed in this paper have been generated on a common personal computer in

less than a day) recommend the application of statistical analog resampling for future regional climate projections as a complement to GCM simulations. Also, the possibility to obtain large ensembles of future projections is a feature reserved to statistical approaches, which allows uncertainty to be evaluated on a stronger basis.

Station data becoming available from China (Xie et al. 2007; Xu et al. 2009) make future climate projections by the statistical analog resampling feasible in this region. Both further developments of STAR and future applications to other parts of China and Eurasia—and their comparison to future RegCM simulations—are envisaged.

Acknowledgments. The authors are grateful to Prof. Qi Steven Hu at the University of Nebraska–Lincoln for providing them with the meteorological station data and to Frank Sielmann at the Institute of Meteorology, University of Hamburg, for compiling the typhoon data. Support by the German Science Foundation DFG-project FR 450/14-2 is acknowledged. B. O. is funded by Research Grant Or 256/1-1 from DFG. Thanks to the Hydrological Bureau of the Yangtze Water Resources Committee (CWRC) for making the runoff data available. Comments from two anonymous reviewers, which helped to substantially improve the manuscript, are gratefully acknowledged.

REFERENCES

Bengtsson, L., K. Hodges, M. Esch, N. Keenlyside, L. Kornblueh, J.-J. Luo, and T. Yamagata, 2007: How may tropical cyclones change in a warmer climate? *Tellus,* **59A,** 539–561.

Bordi, I., and A. Sutera, 2001: Fifty years of precipitation: Some spatially remote teleconnections. *Water Resour. Manage.,* **15,** 247–280.

——, K. Fraedrich, J.-M. Jiang, and A. Sutera, 2004: Spatio-temporal variability of dry and wet periods in eastern China. *Theor. Appl. Climatol.,* **79,** 81–91.

Chan, J., 2005: Interannual and interdecadal variations of tropical cyclone activity over the western North Pacific. *Meteor. Atmos. Phys.,* **89,** 143–152.

Cleveland, R. B., W. S. Cleveland, J. E. McRae, and I. Terpenning, 1990: STL: A seasonal-trend decomposition procedure based on loess. *J. Off. Stat.,* **6,** 3–33.

Davison, A. C., and D. V. Hinkley, 1997: *Bootstrap Methods and Their Application*. Cambridge Series on Statistical and Probabilistic Mathematics, Vol. 1, Cambridge University Press, 582 pp.

Dibike, Y. B., P. Gachon, A. St-Hilaire, T. B. M. J. Ouarda, and V. T.-V. Nguyen, 2008: Uncertainty analysis of statistically downscaled temperature and precipitation regimes in Northern Canada. *Theor. Appl. Climatol.,* **91,** 149–170.

Domrös, M., and P. Gongbing, 1988: *The Climate of China*. Springer-Verlag, 360 pp.

Efron, B., 1979: Bootstrap methods: Another look at the jackknife. *Ann. Stat.,* **7,** 1–26.

——, 1981: Nonparametric standard errors and confidence intervals. *Can. J. Stat.,* **9,** 139–158.

——, and R. J. Tibshirani, 1993: *An Introduction to the Bootstrap.* Monographs on Statistics and Applied Probability, No. 57, Chapman & Hall, 436 pp.

Feng, S., Q. Hu, and W. Qian, 2004: Quality control of daily meteorological data in China, 1951–2000: A new dataset. *Int. J. Climatol.,* **24,** 853–870.

Fraedrich, K., F.-W. Gerstengarbe, and P. C. Werner, 2001: Climate shifts in the last century. *Climatic Change,* **50,** 405–417.

Gao, X., Z. Zhao, and Y. Ding, 2001: Climate Change due to Greenhouse Effects in China as Simulated by a Regional Climate Model. *Adv. Atmos. Sci.,* **18,** 1224–1230.

——, Y. Xu, Z. Zhao, J. S. Pal, and F. Giorgi, 2006: On the role of resolution and topography in the simulation of East Asia precipitation. *Theor. Appl. Climatol.,* **86,** 173–185.

Giorgi, F., 2006: Regional climate modeling: Status and perspectives. *J. Phys. IV,* **139,** 101–118.

——, X. Bi, and J. Pal, 2004: Mean, interannual variability and trends in a regional climate change experiment over Europe. I. Present-day climate (1961–1990). *Climate Dyn.,* **22,** 733–756.

Hagemann, S., K. Arpe, and E. Roeckner, 2006: Evaluation of the hydrological cycle in the ECHAM5 model. *J. Climate,* **19,** 3810–3827.

Hall, P., and B. Presnell, 1999a: Density estimation under constraints. *J. Comput. Graphical Stat.,* **8,** 259–277.

——, and ——, 1999b: Intentionally biased bootstrap methods. *J. Roy. Stat. Soc.,* **61,** 143–158.

Ho, C.-H., J.-J. Baik, J.-H. Kim, D.-Y. Gong, and C.-H. Sui, 2004: Interdecadal changes in summertime typhoon tracks. *J. Climate,* **17,** 1767–1776.

Kotlarski, S., A. Block, U. Böhm, D. Jacob, K. Keuler, R. Knoche, D. Rechid, and A. Walter, 2005: Regional climate model simulations as input for hydrological applications: Evaluation of uncertainties. *Adv. Geosci.,* **5,** 119–125.

Kripalani, R., J. Oh, and H. Chaudhari, 2007: Response of the East Asian summer monsoon to doubled atmospheric CO_2: Coupled climate. *Theor. Appl. Climatol.,* **87,** 1–28.

Lahiri, S. N., 2003: *Resampling Methods for Dependent Data*. Springer Series in Statistics, Springer, 374 pp.

Laprise, R., 2008: Regional climate modelling. *J. Comput. Phys.,* **227,** 3641–3666.

McKee, T. B., N. J. D. Oeskin, and J. K. Kleist, 1993: The relationship of drought frequency and duration to time scales. *Eighth Conf. on Applied Climatology,* Anaheim, CA, Amer. Meteor. Soc., 179–184.

Mudelsee, M., M. Borngen, G. Tetzlaff, and U. Grunewald, 2003: No upward trends in the occurrence of extreme floods in central Europe. *Nature,* **425,** 166–169.

Nakicenovic, N., and R. Swart, Eds., 2000: *IPCC Special Report on Emissions Scenarios*. Cambridge University Press, 599 pp.

Orlowsky, B., and K. Fraedrich, 2009: Upscaling European surface temperatures to North Atlantic circulation-pattern statistics. *Int. J. Climatol.,* **29,** 839–849.

——, F.-W. Gerstengarbe, and P. Werner, 2008: A resampling scheme for regional climate simulations and its performance compared to a dynamical RCM. *Theor. Appl. Climatol.,* **92,** 209–223.

Roeckner, E., and Coauthors, 2003: The atmospheric general circulation model ECHAM 5. PART I: Model description. MPI Tech. Rep. 349, 127 pp.

——, M. Lautenschlager, and H. Schneider, cited 2008a: IPCC-AR4 MPI-ECHAM5_T63L31 MPI-OM_GR1.5L40 20C3M run no.1: Atmosphere 6 hour values MPImet/MaD Germany.

[Available online at http://cera-www.dkrz.de/WDCC/ui/Compact.jsp?acronym=EH5-T63L31_OM-GR1.5L40_20C_1_6H.]

——, ——, and ——, cited 2008b: IPCC-AR4 MPI-ECHAM5_T63L31 MPI-OM_GR1.5L40 SRESA1B run no.1: Atmosphere 6 hour values MPImet/MaD Germany. [Available online at http://cera-www.dkrz.de/WDCC/ui/Compact.jsp?acronym=EH5-T63L31_OM-GR1.5L40_A1B_1_6H.]

Rust, H. W., M. Kallache, H.-J. Schellnhuber, and J. P. Kropp, 2010: Confidence intervals for flood return level estimates assuming long-range dependence. *Extremis: Trends, Correlations, and Extremes in Hydrology and Climate,* J. P. Kropp and H.-J. Schellnhuber, Eds., Springer, in press.

Sienz, F., I. Bordi, K. Fraedrich, and A. Schneidereit, 2007: Extreme dry and wet events in Iceland: Observations, simulations and scenarios. *Meteor. Z.,* **16,** 9–16.

Solomon, S., D. Qin, M. Manning, M. Marquis, K. Averyt, M. M. B. Tignor, H. L. Miller Jr., and Z. Chen, Eds., 2007: *Climate Change 2007: The Physical Science Basis*. Cambridge University Press, 996 pp.

Stowasser, M., Y. Wang, and K. Hamilton, 2007: Tropical cyclone changes in the western North Pacific in a global warming scenario. *J. Climate,* **20,** 2378–2396.

van Oldenborgh, G. J., S. Drijfhout, A. van Ulden, R. Haarsma, A. Sterl, C. Severijns, W. Hazeleger, and H. Dijkstra, 2009: Western Europe is warming much faster than expected. *Climate Past,* **5,** 1–12.

Vautard, R., P. Yiou, and G. J. van Oldenborgh, 2009: Decline of fog, mist and haze in Europe over the past 30 years. *Nat. Geosci.,* **414,** 1–5.

Wang, B., R. Wu, and K.-M. Lau, 2001: Interannual variability of the Asian summer monsoon: Contrasts between the Indian and the western North Pacific–East Asian monsoons. *J. Climate,* **14,** 4073–4090.

Wang, G., T. Jiang, R. Blender, and K. Fraedrich, 2008: Yangtze 1/*f* discharge variability and the interacting river–lake system. *J. Hydrol.,* **351,** 230–237.

Wang, Y., L. R. Leung, D.-K. Lee, W.-C. Wang, Y. Ding, and F. Kimura, 2004: Regional climate modeling: Progress, challenges, and prospects. *J. Meteor. Soc. Japan,* **82,** 1599–1628.

Webster, P., G. Holland, J. Curry, and H.-R. Chang, 2005: Changes in tropical cyclone number, duration, and intensity in a warming environment. *Science,* **309,** 1844–1846.

Werner, P., and F.-W. Gerstengarbe, 1997: Proposal for the development of climate scenarios. *Climate Res.,* **8,** 171–182.

Wilby, R., T. M. L. Wigley, D. Conway, P. D. Jones, B. C. Hewitson, J. Main, and D. S. Wilks, 1998: Statistical downscaling of general circulation model output: A comparison of methods. *Water Resour. Res.,* **34,** 2995–3008.

Wilks, D. S., 1999: Interannual variability and extreme-value characteristics of several stochastic daily precipitation models. *Water Resour. Res.,* **34,** 2995–3008.

Wu, S., Y. Yin, D. Zheng, and Q. Yang, 2006: Moisture conditions and climate trends in China during the period 1971–2000. *Int. J. Climatol.,* **26,** 193–206.

Xie, P., A. Yatagai, M. Chen, T. Hayasaka, Y. Fukushima, C. Liu, and S. Yang, 2007: A gauge-based analysis of daily precipitation over East Asia. *J. Hydrometeor.,* **8,** 607–626.

Xu, C. H., X. Y. Shen, and Y. Xu, 2007: An analysis of climate change in East Asia by using the IPCC AR4 simulations. *Adv. Climate Change Res.,* **3,** 287–292.

Xu, Y., X. Gao, Y. Shen, C. Xu, Y. Shi, and F. Giorgi, 2009: A daily temperature dataset over China and its application in validating a RCM simulation. *Adv. Atmos. Sci.,* **26,** 763–772.

Zorita, E., and H. von Storch, 1999: The analog method as a simple statistical downscaling technique: Comparison with more complicated methods. *J. Climate,* **12,** 2474–2489.